Appl. Math. Mech. -Engl. Ed., **39**(7), 981–992 (2018)

Applied Mathematics and Mechanics (English Edition)

https://doi.org/10.1007/s10483-018-2347-8

Buckling of a sandwich symmetrical circular plate with varying mechanical properties of the core*

E. MAGNUCKA-BLANDZI[1], K. WISNIEWSKA-MLECZKO[2,†], M. J. SMYCZYNSKI[3], P. KEDZIA[3]

1. Institute of Mathematics, Poznan University of Technology, Poznan 60-965, Poland;
2. Department of Engineering and Technology, State University of Applied Sciences in Konin, Konin 62-510, Poland;
3. Institute of Applied Mechanics, Poznan University of Technology, Poznan 60-139, Poland

(Received Oct. 29, 2017 / Revised Feb. 14, 2018)

Abstract This paper is devoted to analytical and numerical studies of global buckling of a sandwich circular plate. The mechanical properties of the plate core vary along its thickness, remaining constant in the facings. The middle surface of the plate is its symmetrical plane. The mathematical model of the plate is presented. The field of displacements is formulated using the proposed nonlinear hypothesis that generalizes the classical hypotheses. The equations of equilibrium are formulated based on the principle of stationary total potential energy. The proposed mathematical model of the displacements considers the shear effect. The numerical model of the plate is also formulated with a view to verify the analytical one. Numerical calculations are carried out for the chosen family of plates. The values of the critical load obtained by the analytical and numerical methods are compared. The effects of the material properties of the core and the change of the plate radius on the critical load intensity are presented.

Key words mathematical modeling, sandwich circular plate, global buckling, critical load

Chinese Library Classification O343
2010 Mathematics Subject Classification 74B05, 74E05, 74K20

Nomenclature

R, radius of the circular plate;
t_c, thickness of the core;
t_f, thickness of the facings;
E_0, Young's modulus in the middle plane of the core;
E_1, Young's modulus at the top and bottom surfaces of the core;
E_f, Young's modulus of the facings;

* Citation: MAGNUCKA-BLANDZI, E., WISNIEWSKA-MLECZKO, K., SMYCZYNSKI, M. J., and KEDZIA, P. Buckling of a sandwich symmetrical circular plate with varying mechanical properties of the core. *Applied Mathematics and Mechanics* (*English Edition*), **39**(7), 981–992 (2018) https://doi.org/10.1007/s10483-018-2347-8

† Corresponding author, E-mail: karolina.sta.wisniewska@doctorate.put.poznan.pl

ν_{c}, Poisson's ratio of the core;
ν_{f}, Poisson's ratio of the facings;
$N_{R,\mathrm{cr}}$, static critical intensity of the load;
U_{ε}, elastic strain energy;
W, work of the load;
w, deflection;
u, longitudinal displacement;
ψ_0, ψ_1, dimensionless functions.

1 Introduction

The global buckling problems of layered structures have been studied since the mid-20th century. When designing layered structures, strength and stability conditions are active constraints. Stability conditions include global buckling problems. A basic theory of sandwich structures is described in the literature[1–4]. Carrera[5] formulated the zig-zag hypotheses for multilayered plates. Carrera and Brischetto[6] presented a survey of the theories for the analysis of sandwich plates. Based on the extensive research, they concluded that the classical lamination theory (CLT) and the first-order shear deformation theory (FSDT) cannot be effectively used for the analysis of sandwich structures. Zenkour[7] derived a refined trigonometric higher-order plate theory for functionally graded plates. Caliri et al.[8] delivered a detailed review of the theories and respective solution methods devoted to laminated and sandwich structures. The solution methods based on the finite element method (FEM) were explained.

The buckling phenomenon was considered in various layer structures such as beams and rectangular, circular, and annular plates. Jasion et al.[9] presented analytical, numerical, and experimental data of the global and local buckling-wrinkling of the face sheets of sandwich beams. Kedzia and Smyczynski[10] studied buckling problems of a three-layer rectangular plate loaded by pockets filled with ferrofluids. Magnucki et al.[11–13] presented analytical investigations of bending and buckling of rectangular plates made of a porous material and sandwich beams. Thai and Choi[14] presented analytical solutions for bending, buckling, and vibration analyses of thick rectangular plates using two variable refined plate theories. Uysal and Güven[15] investigated the buckling behaviors of adhesively bonded sandwich plates subject to the in-plane shear force and the in-plane normal compression force. Magnucka-Blandzi[16–17] presented a mathematical model of a rectangular plate compressed in its middle plane and buckling and bending of the circular plate. Pawlus[18–19] presented the computational results of critical load calculations for annular three-layer plates with a soft core. Alipour and Shariyat[20] presented distributions of in-plane normal and transverse shear stresses for circular/annular sandwich plates with orthotropic composite face sheets and auxetic cores using a zigzag theory whose results are correct based on the three-dimensional theory of elasticity. Magnucki et al.[21] analytically and experimentally studied pure bending of sandwich circular plates. Mao et al.[22] investigated the load carrying capacity of circular sandwich plates subject to the transverse quasi-static point central loading. Mojahedin et al.[23] analyzed the buckling of functionally graded circular plates made of porous materials using the higher-order shear deformation theory. Properties of the porous plate vary across its thickness. The boundary condition of the plate is assumed to be clamped.

The clamped sandwich isotropic circular plate under compression in its middle plane is analyzed. This plate (see Fig. 1) consists of two facings of the thickness t_{f} and the core of the thickness t_{c}. The middle plane of the plate is subject to the load intensity N_R. The radius of the plate equals R. The mechanical properties of the plate core vary along the thickness direction symmetrically with respect to the middle plane of the plate. As a result of the investigation, the mathematical model of the three-layer circular plate is formulated. The results obtained from both analytical and numerical studies using the FEM with the use of SOLIDWORKS system are compared.

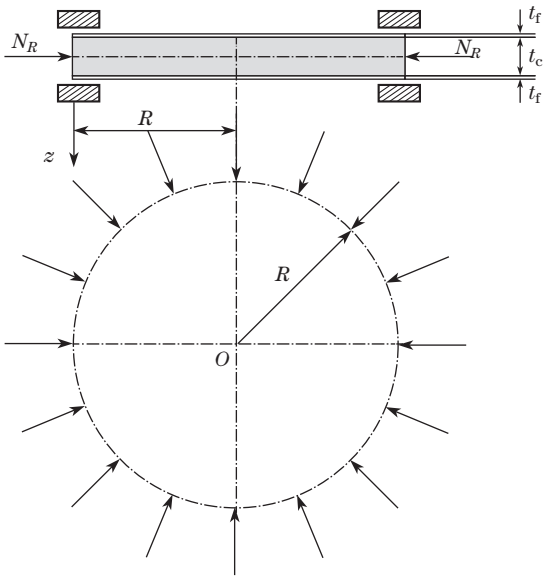

Fig. 1 A schematic of the clamped sandwich circular plate under compression

2 Theoretical models of the circular plate

2.1 Mechanical properties of the plate

The mechanical properties of the core vary through the thickness in the z-direction (see Fig. 2), while the properties of the facings are constant. The middle surface of the plate is its symmetrical plane.

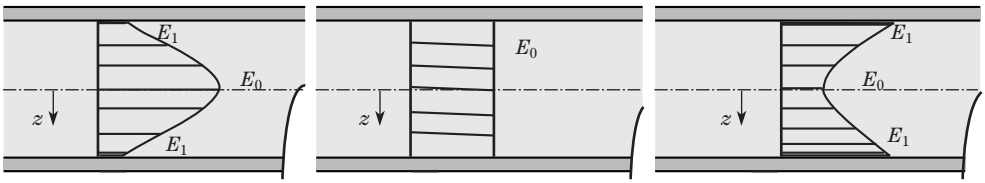

(a) $E_1<E_0$ (b) $E_1=E_0$ (c) $E_1>E_0$

Fig. 2 Variable mechanical properties of the plate core

Young's modulus changes in accordance with the specific function,

$$E_c(z) = E_0 + 4(E_1 - E_0)\left(\frac{z}{t_c}\right)^2, \tag{1}$$

where E_0 is Young's modulus in the middle plane, and E_1 is Young's modulus at the top and bottom surfaces of the core.

There are two particular cases as follows:

(i) if $z = \pm\frac{t_c}{2}$, then $E_c = E_1$;

(ii) if $z = 0$, then $E_c = E_0$.

Young's modulus in the facings E_f is constant. Poisson's ratios in the facings and in the core are also constant.

2.2 The field of displacements

The field of displacements for the global buckling of the sandwich circular plate is shown in Fig. 3, where the displacements $u(r, z)$ and $u_f(r)$ are presented. The adapted Mindlin-Reissner

hypothesis for three-layer plates is presented in Fig. 3(a), while the proposed nonlinear one is shown in Fig. 3(b). These hypotheses include the shear effect and generalize the classical Kirchhoff-Love hypothesis which neglects the shear effect.

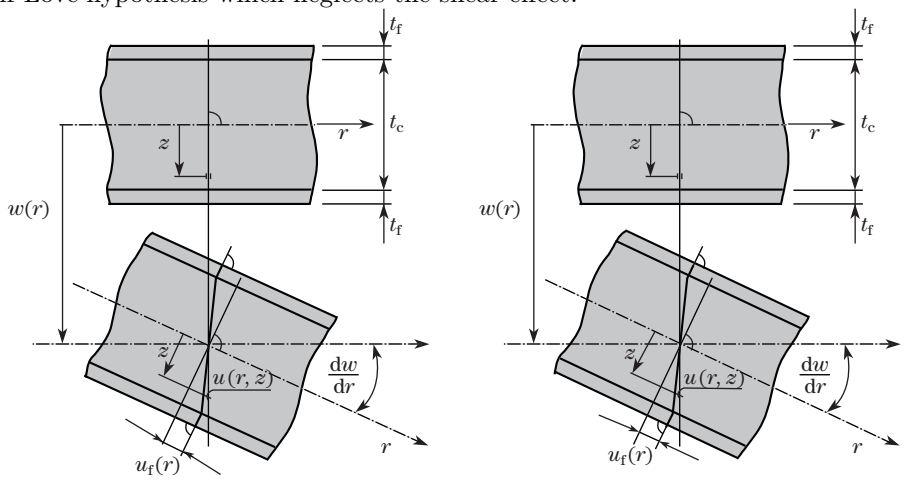

Fig. 3 Schematics of displacements for the plate of (a) the adapted Mindlin-Reissner hypothesis and (b) the proposed nonlinear hypothesis

According to Fig. 3, the displacements in the case of the nonlinear hypothesis are as follows:
(i) for the upper layer, $-(\frac{t_c}{2}+t_f) \leqslant z \leqslant -\frac{t_c}{2}$,

$$u(r,z) = -z\Big(\frac{dw}{dr} + \frac{t_c}{z}\psi_0(r)\Big);$$

(ii) for the core, $-\frac{t_c}{2} \leqslant z \leqslant \frac{t_c}{2}$,

$$u(r,z) = -z\Big(\frac{dw}{dz} - 2\psi_0(r) + \Big(\Big(\frac{2z}{t_c}\Big)^2 - 1\Big)\psi_1(r)\Big);$$

(iii) for the lower layer, $\frac{t_c}{2} \leqslant z \leqslant \frac{t_c}{2}+t_f$,

$$u(r,z) = -z\Big(\frac{dw}{dr} - \frac{t_c}{z}\psi_0(r)\Big),$$

where $\psi_0(r) = u_f(r)/t_c$.

The proposed nonlinear hypothesis is a generalization of the Mindlin-Reissner hypothesis. In the particular case when the function $\psi_1(r) \equiv 0$, the above field of displacements describes the adapted Mindlin-Reissner hypothesis. If the functions $\psi_0(r) \equiv 0$ and $\psi_1(r) \equiv 0$, the above field of displacements describes the Kirchhoff-Love hypothesis. If these functions are not equal to zero, then one obtains the nonlinear hypothesis.

Based on the displacements, the strains and stresses are determined.

The strains (ε is the normal strain, and γ is the shear strain) are as follows:
(i) for the upper layer (the upper facing),

$$\varepsilon_r^{(uf)} = -\Big(z\frac{d^2w}{dr^2} + t_c\frac{d\psi_0}{dr}\Big),$$

$$\varepsilon_\varphi^{(uf)} = -\frac{1}{r}\Big(z\frac{dw}{dr} + t_c\psi_0(r)\Big),$$

$$\gamma_{rz}^{(uf)} = 0;$$

(ii) for the core,

$$\varepsilon_r^{(\mathrm{c})} = -z\Big(\frac{\mathrm{d}^2 w}{\mathrm{d}r^2} - 2\frac{\mathrm{d}\psi_0}{\mathrm{d}r} + \Big(\Big(\frac{2z}{t_\mathrm{c}}\Big)^2 - 1\Big)\frac{\mathrm{d}\psi_0}{\mathrm{d}r}\Big),$$
$$\varepsilon_\varphi^{(\mathrm{c})} = -\frac{z}{r}\Big(\frac{\mathrm{d}w}{\mathrm{d}r} - 2\psi_0(r) + \Big(\Big(\frac{2z}{t_\mathrm{c}}\Big)^2 - 1\Big)\psi_1(r)\Big),$$
$$\gamma_{rz}^{(\mathrm{c})} = 2\psi_0 - \Big(3z^2\Big(\frac{2}{t_\mathrm{c}}\Big)^2 - 1\Big)\psi_1(r);$$

(iii) for the lower layer (the lower facing),

$$\varepsilon_r^{(\mathrm{lf})} = -\Big(z\frac{\mathrm{d}^2 w}{\mathrm{d}r^2} - t_\mathrm{c}\frac{\mathrm{d}\psi_0}{\mathrm{d}r}\Big),$$
$$\varepsilon_\varphi^{(\mathrm{lf})} = -\frac{1}{r}\Big(z\frac{\mathrm{d}w}{\mathrm{d}r} - t_\mathrm{c}\psi_0(r)\Big),$$
$$\gamma_{rz}^{(\mathrm{lf})} = 0.$$

The stresses (σ is the normal stress, and τ is the shear stress) are as follows:
(i) for the facings,

$$\sigma_r = \frac{E_\mathrm{f}}{1-\nu_\mathrm{f}^2}(\varepsilon_r + \nu_\mathrm{f}\varepsilon_\varphi),$$
$$\sigma_\varphi = \frac{E_\mathrm{f}}{1-\nu_\mathrm{f}^2}(\varepsilon_\varphi + \nu_\mathrm{f}\varepsilon_r),$$
$$\tau_{rz} = G\gamma_{rz} = 0;$$

(ii) for the core,

$$\sigma_r^{(\mathrm{c})} = \frac{\varepsilon_r + \nu_\mathrm{c}\varepsilon_\varphi}{1-\nu_\mathrm{c}^2}\Big(E_0 + 4(E_1 - E_0)\Big(\frac{z}{t_\mathrm{c}}\Big)^2\Big),$$
$$\sigma_\varphi^{(\mathrm{c})} = \frac{\varepsilon_\varphi + \nu_\mathrm{c}\varepsilon_r}{1-\nu_\mathrm{c}^2}\Big(E_0 + 4(E_1 - E_0)\Big(\frac{z}{t_\mathrm{c}}\Big)^2\Big),$$
$$\tau_{rz}^{(\mathrm{c})} = \frac{1}{2(1+\nu_\mathrm{c})}\Big(E_0 + 4(E_1 - E_0)\Big(\frac{z}{t_\mathrm{c}}\Big)^2\Big)\Big(2\psi_0 - \Big(3\Big(\frac{2z}{t_\mathrm{c}}\Big)^2 - 1\Big)\psi_1\Big),$$

where ν_f is Poisson's ratio of the facings, and ν_c is Poisson's ratio of the core.

3 Equilibrium equations

Based on the principle of the total potential energy,

$$\delta(U_\varepsilon - W) = 0, \tag{2}$$

the system of equilibrium equations has been obtained, where the work of the load is

$$W = \pi N_R \int_0^R \Big(\frac{\mathrm{d}w}{\mathrm{d}r}\Big)^2 r\mathrm{d}r, \tag{3}$$

and the elastic strain energy is

$$U_\varepsilon = U_\varepsilon^{(\mathrm{uf})} + U_\varepsilon^{(\mathrm{c})} + U_\varepsilon^{(\mathrm{lf})}, \tag{4}$$

where $U_\varepsilon^{(\mathrm{uf})}$ is the elastic strain energy of the upper facing,

$$U_\varepsilon^{(\mathrm{uf})} = \pi \int_0^R \int_{-(t_\mathrm{c}/2+t_\mathrm{f})}^{-t_\mathrm{c}/2} (\varepsilon_r^{(\mathrm{uf})}\sigma_r^{(\mathrm{uf})} + \varepsilon_\varphi^{(\mathrm{uf})}\sigma_\varphi^{(\mathrm{uf})} + \tau_{rz}^{(\mathrm{uf})}\gamma_{rz}^{(\mathrm{uf})})r\mathrm{d}z\mathrm{d}r,$$

$U_{\varepsilon}^{(\mathrm{c})}$ is the elastic strain energy of the core,

$$U_{\varepsilon}^{(\mathrm{c})} = \pi \int_0^R \int_{-t_\mathrm{c}/2}^{t_\mathrm{c}/2} (\varepsilon_r^{(\mathrm{c})}\sigma_r^{(\mathrm{c})} + \varepsilon_\varphi^{(\mathrm{c})}\sigma_\varphi^{(\mathrm{c})} + \tau_{rz}^{(\mathrm{c})}\gamma_{rz}^{(\mathrm{c})}) r \mathrm{d}z\mathrm{d}r,$$

and $U_{\varepsilon}^{(\mathrm{lf})}$ is the elastic strain energy of the lower facing,

$$U_{\varepsilon}^{(\mathrm{lf})} = \pi \int_0^R \int_{t_\mathrm{c}/2}^{t_\mathrm{c}/2+t_\mathrm{f}} (\varepsilon_r^{(\mathrm{lf})}\sigma_r^{(\mathrm{lf})} + \varepsilon_\varphi^{(\mathrm{lf})}\sigma_\varphi^{(\mathrm{lf})} + \tau_{rz}^{(\mathrm{lf})}\gamma_{rz}^{(\mathrm{lf})}) r \mathrm{d}z\mathrm{d}r.$$

Then, the system of equilibrium equations is as follows:

$$\begin{cases} \dfrac{E_\mathrm{f} t_\mathrm{c}^3}{1-\nu_\mathrm{f}^2}\Big(A_{11}\Big(r\dfrac{\mathrm{d}^4 w}{\mathrm{d}r^4} + 2\dfrac{\mathrm{d}^3 w}{\mathrm{d}r^3} - \dfrac{1}{r}\dfrac{\mathrm{d}^2 w}{\mathrm{d}r^2} + \dfrac{1}{r^2}\dfrac{\mathrm{d}w}{\mathrm{d}r}\Big) - A_{12}\Big(r\dfrac{\mathrm{d}^3\psi_0}{\mathrm{d}r^3} + 2\dfrac{\mathrm{d}^2\psi_0}{\mathrm{d}r^2} - \dfrac{1}{r}\dfrac{\mathrm{d}\psi_0}{\mathrm{d}r} \\ + \dfrac{1}{r^2}\psi_0\Big) - B_{13}\Big(r\dfrac{\mathrm{d}^3\psi_1}{\mathrm{d}r^3} + 2\dfrac{\mathrm{d}^2\psi_1}{\mathrm{d}r^2} - \dfrac{1}{r}\dfrac{\mathrm{d}\psi_1}{\mathrm{d}r} + \dfrac{1}{r^2}\psi_1\Big)\Big) = -2N_R\Big(\dfrac{\mathrm{d}w}{\mathrm{d}r} + r\dfrac{\mathrm{d}^2 w}{\mathrm{d}r^2}\Big), \\ \dfrac{t_\mathrm{c}^2}{1-\nu_\mathrm{f}^2}\Big(A_{12}\Big(r\dfrac{\mathrm{d}^3 w}{\mathrm{d}r^3} + \dfrac{\mathrm{d}^2 w}{\mathrm{d}r^2} - \dfrac{1}{r}\dfrac{\mathrm{d}w}{\mathrm{d}r}\Big) - A_{22}\Big(r\dfrac{\mathrm{d}^2\psi_0}{\mathrm{d}r^2} + \dfrac{\mathrm{d}\psi_0}{\mathrm{d}r} - \dfrac{1}{r}\psi_0\Big) \\ - B_{23}\Big(r\dfrac{\mathrm{d}^2\psi_1}{\mathrm{d}r^2} + \dfrac{\mathrm{d}\psi_1}{\mathrm{d}r} - \dfrac{1}{r}\psi_1\Big)\Big) + A_{24} r\psi_0 + B_{25} r\psi_1 = 0, \\ \dfrac{t_\mathrm{c}^2}{1-\nu_\mathrm{f}^2}\Big(B_{13}\Big(r\dfrac{\mathrm{d}^3 w}{\mathrm{d}r^3} + \dfrac{\mathrm{d}^2 w}{\mathrm{d}r^2} - \dfrac{1}{r}\dfrac{\mathrm{d}w}{\mathrm{d}r}\Big) - B_{23}\Big(r\dfrac{\mathrm{d}^2\psi_0}{\mathrm{d}r^2} + \dfrac{\mathrm{d}\psi_0}{\mathrm{d}r} - \dfrac{1}{r}\psi_0\Big) \\ - B_{33}\Big(r\dfrac{\mathrm{d}^2\psi_1}{\mathrm{d}r^2} + \dfrac{\mathrm{d}\psi_1}{\mathrm{d}r} - \dfrac{1}{r}\psi_1\Big)\Big) + B_{25} r\psi_0 + B_{35} r\psi_1 = 0, \end{cases} \tag{5}$$

where

$$\alpha_1 = \frac{1}{12}(3 + 6x_1 + 4x_1^2)x_1, \quad \alpha_2 = \frac{1}{2}x_1(1+x_1), \quad \beta_1 = \frac{1-\nu_\mathrm{f}^2}{1-\nu_\mathrm{c}^2}, \quad x_1 = \frac{t_\mathrm{f}}{t_\mathrm{c}},$$

$$A_{11} = 4\alpha_1 + \frac{1}{30}\beta_1\frac{2E_0+3E_1}{E_\mathrm{f}}, \quad A_{12} = 4\alpha_2 + \frac{1}{15}\beta_1\frac{2E_0+3E_1}{E_\mathrm{f}}, \quad A_{21} = A_{12},$$

$$A_{22} = 4x_1 + \frac{2}{15}\beta_1\frac{2E_0+3E_1}{E_\mathrm{f}}, \quad A_{24} = \frac{4}{3}\frac{1}{1+\nu_\mathrm{c}}\frac{2E_0+E_1}{E_\mathrm{f}}, \quad B_{13} = \frac{1}{105}\beta_1\frac{4E_0+3E_1}{E_\mathrm{f}},$$

$$B_{23} = \frac{2}{105}\beta_1\frac{4E_0+3E_1}{E_\mathrm{f}}, \quad B_{25} = \frac{8}{15}\frac{1}{1+\nu_\mathrm{c}}\frac{E_0-E_1}{E_\mathrm{f}}, \quad B_{31} = B_{13},$$

$$B_{32} = B_{23}, \quad B_{33} = \frac{4}{315}\beta_1\frac{2E_0+E_1}{E_\mathrm{f}}, \quad B_{34} = B_{25}, \quad B_{35} = \frac{4}{105}\frac{1}{1+\nu_\mathrm{c}}\frac{10E_0+11E_1}{E_\mathrm{f}},$$

$$C_{11} = \frac{1}{2}A_{22} + \frac{2}{15}A_{24}\Big(\frac{R}{t_\mathrm{c}}\Big)^2(1-\nu_\mathrm{f}^2), \quad C_{12} = \frac{1}{2}B_{23} + \frac{2}{15}B_{25}\Big(\frac{R}{t_\mathrm{c}}\Big)^2(1-\nu_\mathrm{f}^2),$$

$$C_{22} = \frac{1}{2}B_{33} + \frac{2}{15}B_{35}\Big(\frac{R}{t_\mathrm{c}}\Big)^2(1-\nu_\mathrm{f}^2).$$

4 Analytical solutions

The system (5) has three unknown functions (w is the deflection, and ψ_0 and ψ_1 are dimensionless functions that determine the normal deformations in the middle plane of the plate).

Then, the following formulas for these functions are assumed:

$$\begin{cases} w(r) = w_{\mathrm{a}}\Big(1 - 3\Big(\dfrac{r}{R}\Big)^2 + 2\Big(\dfrac{r}{R}\Big)^3\Big), \\ \psi_0(r) = \psi_{\mathrm{a}0}\Big(\dfrac{r}{R} - \dfrac{1}{2}\Big(\dfrac{r}{R}\Big)^2\Big), \\ \psi_1(r) = \psi_{\mathrm{a}1}\Big(\dfrac{r}{R} - \dfrac{1}{2}\Big(\dfrac{r}{R}\Big)^2\Big), \end{cases} \tag{6}$$

which identically satisfy the boundary conditions when the plate is clamped at its edge for $r = R$,

$$w(R) = 0, \quad \frac{\mathrm{d}w}{\mathrm{d}r}\Big|_{r=R} = 0, \tag{7}$$

and the condition in the middle of the plate for $r = 0$,

$$\frac{\mathrm{d}w}{\mathrm{d}r}\Big|_{r=0} = 0, \tag{8}$$

where w_{a} is the amplitude of deflection, and $\psi_{\mathrm{a}0}$ and $\psi_{\mathrm{a}1}$ are amplitudes of dimensionless functions, respectively. By substituting (6) to the system (5) and using the Bubnov-Galerkin method, the system (5) takes the form of

$$\begin{cases} \dfrac{E_{\mathrm{f}} t_{\mathrm{c}}^3}{1-\nu_{\mathrm{f}}^2}\Big(6A_{11}\dfrac{w_{\mathrm{a}}}{R} + \dfrac{1}{2}A_{12}\psi_{\mathrm{a}0} + \dfrac{1}{2}B_{13}\psi_{\mathrm{a}1}\Big) - \dfrac{4}{5}N_R w_{\mathrm{a}} R = 0, \\ \dfrac{t_{\mathrm{c}}^2}{1-\nu_{\mathrm{f}}^2}\dfrac{1}{R^2}\Big(6A_{12}\dfrac{w_{\mathrm{a}}}{R} + \dfrac{1}{2}A_{22}\psi_{\mathrm{a}0} + \dfrac{1}{2}B_{23}\psi_{\mathrm{a}1}\Big) + \dfrac{2}{15}(A_{24}\psi_{\mathrm{a}0} + B_{25}\psi_{\mathrm{a}1}) = 0, \\ \dfrac{t_{\mathrm{c}}^2}{1-\nu_{\mathrm{f}}^2}\dfrac{1}{R^2}\Big(6B_{13}\dfrac{w_{\mathrm{a}}}{R} + \dfrac{1}{2}B_{23}\psi_{\mathrm{a}0} + \dfrac{1}{2}B_{33}\psi_{\mathrm{a}1}\Big) + \dfrac{2}{15}(B_{25}\psi_{\mathrm{a}0} + B_{35}\psi_{\mathrm{a}1}) = 0. \end{cases} \tag{9}$$

The functions $\psi_{\mathrm{a}0}$ and $\psi_{\mathrm{a}1}$ are obtained from the second and third equations of the system (9),

$$\psi_{\mathrm{a}0} = \widetilde{\psi}_{\mathrm{a}0}\frac{w_{\mathrm{a}}}{R}, \quad \psi_{\mathrm{a}1} = \widetilde{\psi}_{\mathrm{a}1}\frac{w_{\mathrm{a}}}{R}, \tag{10}$$

where

$$\widetilde{\psi}_{\mathrm{a}0} = 6\frac{C_{12}B_{13} - C_{22}A_{12}}{C_{11}C_{22} - C_{12}^2}, \quad \widetilde{\psi}_{\mathrm{a}1} = 6\frac{C_{12}A_{12} - C_{11}B_{13}}{C_{11}C_{22} - C_{12}^2}. \tag{11}$$

After substituting (10) into the first equation of the system (9), the intensity of critical loads is obtained as

$$N_{R,\mathrm{cr}}^{\mathrm{n}} = \frac{5}{8}\frac{E_{\mathrm{f}} t_{\mathrm{c}}}{1-\nu_{\mathrm{f}}^2}\Big(\frac{t_{\mathrm{c}}}{R}\Big)^2(12A_{11} + A_{12}\widetilde{\psi}_{\mathrm{a}0} + B_{13}\widetilde{\psi}_{\mathrm{a}1}), \tag{12}$$

which is related to the proposed nonlinear hypothesis.

5 Numerical calculations

Critical loads are calculated numerically for a family of the plates. Numerical calculations are conducted using the FEM with SOLIDWORKS. The plate is clamped at the outer edge and loaded, as shown in Fig. 1. A quarter of the circular plate is modeled because of its symmetry (see Fig. 4). The model consists of three layers, two facings and the core. The core is divided into 9 layers (see Fig. 5(b)) with the same thicknesses and different mechanical properties, according to (1). The integrated system component for analyzing composites has been used in calculations. In consequence, all the layers have been modeled as shell elements, and the tie

conditions between the layers have been imposed automatically. Figure 5(b) shows the division of the plate core into layers. The properties of the plate core have been changed according to the relationship shown in Fig. 2. The finite element mesh of the plate is presented in Fig. 5(a). The buckling analysis of the plate under compression has been performed with a view to obtain the intensity of critical loads. A quarter of the buckled plate is presented in Fig. 6 (the first mode is the global buckling mode).

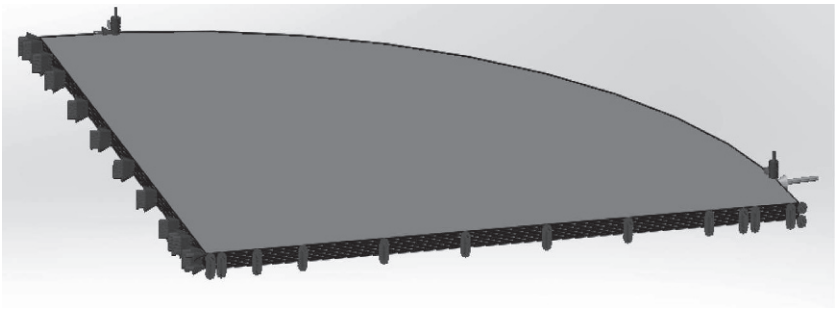

Fig. 4 A quarter of the circular plate and its support

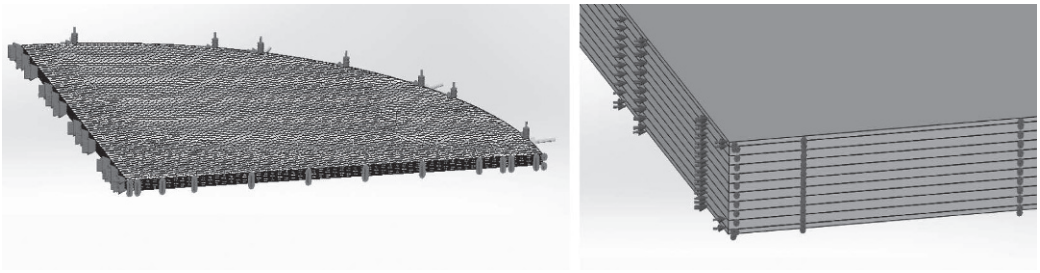

(a) (b)

Fig. 5 The FEM model with (a) the finite element mesh of the plate and (b) the division of the core into 9 layers

Fig. 6 A quarter of the buckled plate using the FEM

The analytical and numerical calculations are carried out for a family of plates with the following parameters: $t_{\mathrm{f}} = 1$ mm, $t_{\mathrm{c}} = 18$ mm, $900\,\mathrm{mm} < R < 2\,250\,\mathrm{mm}$, $E_{\mathrm{f}} = 65\,600$ MPa, $E_0 = 500$ MPa, and $\nu_{\mathrm{f}} = \nu_{\mathrm{c}} = 0.3$.

The values of the intensity of critical loads obtained both analytically and numerically are presented in Table 1 for different values of the parameter $e_{10} = E_1/E_0$ when $\lambda = 50$, where analytical $N^{\mathrm{n}}_{R,\mathrm{cr}}$, $N^{\mathrm{M\text{-}R}}_{R,\mathrm{cr}}$, and $N^{\mathrm{K\text{-}L}}_{R,\mathrm{cr}}$ represent results of the nonlinear hypothesis, the adapted

Mindlin-Reissner hypothesis, and the Kirchhoff-Love hypothesis, respectively, $N_{R,\mathrm{cr}}^{\mathrm{FEM}}$ is the numerical result, and $\lambda = R/t_{\mathrm{c}}$.

In addition, the relative difference (R_{d}) between these values is obtained as

$$R_{\mathrm{d}} = \frac{|N_{R,\mathrm{cr}}^{\mathrm{n}} - N_{R,\mathrm{cr}}^{\mathrm{FEM}}|}{\min\{N_{R,\mathrm{cr}}^{\mathrm{n}}, N_{R,\mathrm{cr}}^{\mathrm{FEM}}\}}.$$

Table 1 Critical loads $N_{R,\mathrm{cr}}$ when $\lambda = 50$

e_{10}	0.2	0.4	0.6	0.8	**1.0**	1.2	1.4	1.6	1.8	2.0
$N_{R,\mathrm{cr}}^{\mathrm{K\text{-}L}}/(\mathrm{N\cdot mm^{-1}})$	243.75	244.35	244.94	245.53	**246.12**	246.72	247.31	247.91	248.50	249.10
$N_{R,\mathrm{cr}}^{\mathrm{M\text{-}R}}/(\mathrm{N\cdot mm^{-1}})$	237.86	239.33	240.45	241.40	**242.26**	243.06	243.82	244.56	245.27	245.97
$N_{R,\mathrm{cr}}^{\mathrm{n}}/(\mathrm{N\cdot mm^{-1}})$	237.87	239.34	240.45	241.40	**242.26**	243.06	243.82	244.55	245.26	245.96
$N_{R,\mathrm{cr}}^{\mathrm{FEM}}/(\mathrm{N\cdot mm^{-1}})$	237.39	237.94	238.50	239.07	**239.63**	240.18	240.75	241.31	241.86	242.43
$R_{\mathrm{d}}/\%$	0.2	0.6	0.8	1.0	**1.1**	1.2	1.3	1.3	1.4	1.5

The values of the intensity of critical loads obtained both analytically and numerically for different values of the parameter $e_{10} = E_1/E_0$ when $\lambda = 75$ are presented in Table 2.

Table 2 Critical loads $N_{R,\mathrm{cr}}$ when $\lambda = 75$

e_{10}	0.2	0.4	0.6	0.8	**1.0**	1.2	1.4	1.6	1.8	2.0
$N_{R,\mathrm{cr}}^{\mathrm{K\text{-}L}}/(\mathrm{N\cdot mm^{-1}})$	108.34	108.60	108.86	109.13	**109.39**	109.65	109.92	110.18	110.45	110.71
$N_{R,\mathrm{cr}}^{\mathrm{M\text{-}R}}/(\mathrm{N\cdot mm^{-1}})$	107.15	107.60	107.97	108.30	**108.62**	108.93	109.22	109.51	109.80	110.09
$N_{R,\mathrm{cr}}^{\mathrm{n}}/(\mathrm{N\cdot mm^{-1}})$	107.16	107.60	107.97	108.30	**108.62**	108.92	109.22	109.51	109.80	110.08
$N_{R,\mathrm{cr}}^{\mathrm{FEM}}/(\mathrm{N\cdot mm^{-1}})$	105.82	106.07	106.32	106.57	**106.82**	107.07	107.32	107.56	107.81	108.06
$R_{\mathrm{d}}/\%$	1.2	1.4	1.5	1.6	**1.7**	1.7	1.8	1.8	1.8	1.9

The values with the bold font (see Tables 1 and 2) correspond to the core with the constant mechanical properties ($e_{10} = 1$ means $E_1 = E_0$, then, Young's modulus is constant in the plate core). If $e_{10} \neq 1$, then the values of the intensity of critical loads correspond to the plate core with variable mechanical properties. The expression (12) which is a function of the intensity of critical loads obtained analytically is a solid line presented in Fig. 7, whereas the values obtained numerically (given in Tables 1 and 2) are marked by dots. It can be observed that, if the parameter e_{10} increases, then the intensity of critical loads also increases. The largest difference between the intensity of critical loads, given by analytical and FEM calculations for $e_{10} = 2$ (see Tables 1 and 2), does not exceed 1.9% in the case of the nonlinear hypothesis. For the Kirchhoff-Love hypothesis, the difference is about 2.8%. The relative differences between the analytical and numerical results increase (see Tables 1 and 2 and Fig. 7) with the increase in e_{10}.

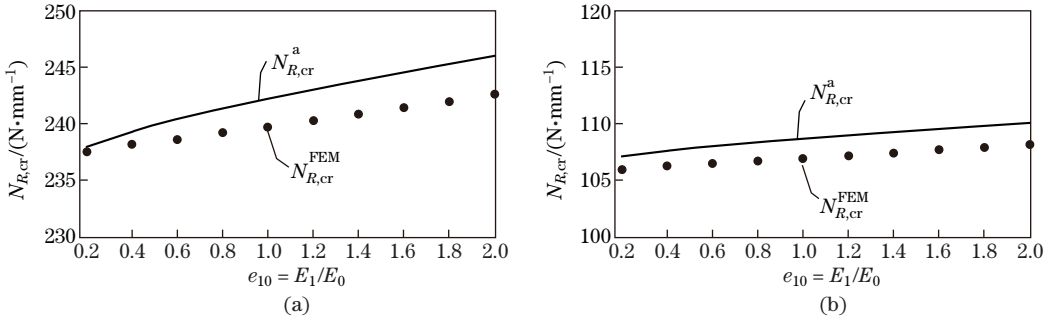

Fig. 7 Comparisons of the analytical and FEM results for (a) $\lambda = 50$ and (b) $\lambda = 75$, where $N_{R,\mathrm{cr}}^{\mathrm{a}}$ and $N_{R,\mathrm{cr}}^{\mathrm{FEM}}$ represent analytical results and numerical results, respectively

The values of the intensity of critical loads obtained with these methods when $\lambda = 100$ and the relative difference between these results are presented in Table 3.

Table 3 Critical loads $N_{R,\mathrm{cr}}$ when $\lambda = 100$

e_{10}	0.2	0.4	0.6	0.8	**1.0**	1.2	1.4	1.6	1.8	2.0
$N^{\mathrm{K\text{-}L}}_{R,\mathrm{cr}}/(\mathrm{N\cdot mm^{-1}})$	60.94	61.09	61.24	61.38	**61.53**	61.68	61.83	61.98	62.13	62.27
$N^{\mathrm{M\text{-}R}}_{R,\mathrm{cr}}/(\mathrm{N\cdot mm^{-1}})$	60.56	60.77	60.95	61.12	**61.29**	61.45	61.61	61.77	61.92	62.08
$N^{\mathrm{n}}_{R,\mathrm{cr}}/(\mathrm{N\cdot mm^{-1}})$	60.56	60.77	60.95	61.12	**61.29**	61.45	61.61	61.77	61.92	62.08
$N^{\mathrm{FEM}}_{R,\mathrm{cr}}/(\mathrm{N\cdot mm^{-1}})$	59.58	59.72	59.86	60.00	**60.14**	60.28	60.42	60.56	60.70	60.84
$R_{\mathrm{d}}/\%$	1.6	1.7	1.8	1.8	**1.9**	1.9	2.0	2.0	2.0	2.0

The values with the bold font (see Table 3) also correspond to the core with constant mechanical properties ($e_{10} = 1$). It can also be observed that the intensity of critical loads increases for the increasing parameter e_{10}.

The values of the intensity of critical loads obtained with these methods when $\lambda = 125$ are presented in Table 4.

Table 4 Critical loads $N_{R,\mathrm{cr}}$ when $\lambda = 125$

e_{10}	0.2	0.4	0.6	0.8	**1.0**	1.2	1.4	1.6	1.8	2.0
$N^{\mathrm{K\text{-}L}}_{R,\mathrm{cr}}/(\mathrm{N\cdot mm^{-1}})$	39.00	39.10	39.19	39.29	**39.38**	39.48	39.57	39.67	39.76	39.86
$N^{\mathrm{M\text{-}R}}_{R,\mathrm{cr}}/(\mathrm{N\cdot mm^{-1}})$	38.85	38.96	39.07	39.18	**39.28**	39.38	39.48	39.58	39.68	39.77
$N^{\mathrm{n}}_{R,\mathrm{cr}}/(\mathrm{N\cdot mm^{-1}})$	38.85	38.97	39.07	39.18	**39.28**	39.38	39.48	39.58	39.68	39.77
$N^{\mathrm{FEM}}_{R,\mathrm{cr}}/(\mathrm{N\cdot mm^{-1}})$	38.15	38.24	38.33	38.42	**38.51**	38.60	38.69	38.78	38.87	38.96
$R_{\mathrm{d}}/\%$	1.8	1.9	1.9	2.0	**2.0**	2.0	2.0	2.1	2.1	2.1

The obtained results when $\lambda = 100$ and $\lambda = 125$ are illustrated in Fig. 8. The analytical results (the expression (12) is a function of the intensity of critical loads) and the numerical ones (the values of the intensity of critical loads for selected parameters e_{10}) are presented in Fig. 8 when $\lambda = 100$ and $\lambda = 125$. The solid lines correspond to the analytical solutions, while the dots correspond to the numerical ones. It can be noticed that the intensity of critical loads increases for the growing parameter e_{10}. The largest difference between the intensity of critical loads given by analytical and FEM calculations is about 2% in the case of the nonlinear hypothesis and occurs for $e_{10} = 2$ (see Tables 3 and 4). The difference between the analytical and numerical results is larger for larger values of λ (see Tables 1–4). The relative differences with the analytical and numerical results are almost the same when $\lambda = 125$, while for smaller values of λ, these differences increase (see Tables 1 and 2 and Fig. 7) for the increasing value e_{10}. For the constant mechanical properties of the core ($e_{10} = 1$ that means $E_1 = E_0$), the difference between the numerical and analytical results is the smallest when $\lambda = 50$ (about 1%

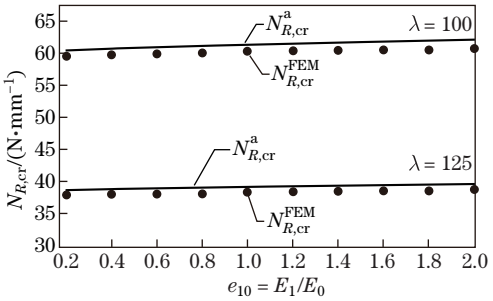

Fig. 8 Comparisons of the analytical and FEM results when $\lambda = 100$ and $\lambda = 125$, where $N^{\mathrm{a}}_{R,\mathrm{cr}}$ and $N^{\mathrm{FEM}}_{R,\mathrm{cr}}$ represent analytical results and numerical results, respectively

in the case of the nonlinear hypothesis) and grows for increasing λ (about 2% in the case of the nonlinear hypothesis when $\lambda = 125$).

6 Conclusions

The mathematical and numerical models of sandwich circular plates are presented, which makes it possible to investigate the influence of the material properties of the core on the critical load intensity. Numerical calculations for a family of plates are performed not only using the analytical formula obtained in the paper but also with the FEM method. Based on the analysis, the following conclusions can be drawn:

(I) If the parameter e_{10} increases, then the intensity of critical loads increases.

(II) If the radius of the plate R increases (if the parameter λ increases), then the intensity of critical loads decreases.

(III) There are small discrepancies between the analytical and numerical results.

(IV) The largest difference between the results obtained numerically and analytically is about 2%.

(V) The smallest change of critical load intensity induced by varying the parameter e_{10} occurs for the largest λ (the largest plate radius).

The choice of the hypothesis does not significantly affect the intensity of critical loads in the case of symmetrical sandwich structures.

The proposed nonlinear hypothesis generalizing the Mindlin-Reissner hypothesis takes into account the shearing effect. Thus, significant differences will be noticeable in the distribution of shear stresses for symmetric sandwich structures.

Acknowledgements The research was carried out within the statutory activities of the Ministry of Science and Higher Education.

References

[1] LIBOVE, C. and BUTDORF, S. B. *A General Small-Deflection Theory for Flat Sandwich Plates*, National Advisory Committee for Aeronautics, Washington, D. C. (1948)

[2] REISSNER, E. Finite deflections of sandwich plates. *Journal of the Aeronautical Sciences*, **15**, 435–440 (1948)

[3] PLANTEMA, F. J. *Sandwich Construction*: *the Bending and Buckling of Sandwich Beams*, *Plates and Shells*, John Wiley and Sons, New York (1966)

[4] ALLEN, H. G. *Analysis and Design of Structural Sandwich Panels*, Pergamon Press, Oxford (1969)

[5] CARRERA, E. An assessment of mixed and classical theories on global and local response of multilayered orthotropic plates. *Composite Structures*, **50**, 183–198 (2000)

[6] CARRERA, E. and BRISCHETTO, S. A survey with numerical assessment of classical and refined theories for the analysis of sandwich plates. *Applied Mechanics Reviews*, **62**, 010803 (2009)

[7] ZENKOUR, A. M. A simple four-unknown refined theory for bending analysis of functionally graded plates. *Applied Mathematical Modelling*, **37**, 9041–9051 (2013)

[8] CALIRI, M. F., JR., FERREIRA, A. J. M., and TITA, V. A review on plate and shell theories for laminated and sandwich structures highlighting the finite element method. *Composite Structures*, **156**, 63–77 (2016)

[9] JASION, P., MAGNUCKA-BLANDZI, E., SZYC, W., and MAGNUCKI, K. Global and local buckling of sandwich circular and beam-rectangular plates with metal foam core. *Thin-Walled Structures*, **61**, 154–161 (2012)

[10] KEDZIA, P. and SMYCZYNSKI, M. J. Homogeneity of magnetic field influence on buckling of three layer polyethylene plate. *Composite Structures*, **183**, 331–337 (2018)

[11] MAGNUCKI, K., MALINOWSKI, M., and KASPRZAK, J. Bending and buckling of a rectangular porous plate. *Steel and Composite Structures*, **6**, 319–333 (2006)

[12] MAGNUCKI, K., JASION, P., SZYC, W., and SMYCZYNSKI, M. J. Strength and buckling of a sandwich beam with thin binding layers between faces and a metal foam core. *Steel and Composite Structures*, **16**, 325–337 (2014)

[13] MAGNUCKI, K., SMYCZYNSKI, M. J., and JASION, P. Deflection and strength of a sandwich beam with thin binding layers between faces and a core. *Archives of Mechanics*, **65**, 301–311 (2013)

[14] THAI, H. T. and CHOI, D. H. Analytical solutions of refined plate theory for bending, buckling and vibration analyses of thick plates. *Applied Mathematical Modelling*, **37**, 8310–8323 (2013)

[15] UYSAL, U. M. and GÜVEN, U. Buckling of functional graded polymeric sandwich panel under different load cases. *Composite Structures*, **121**, 182–196 (2015)

[16] MAGNUCKA-BLANDZI, E. Mathematical modeling of a rectangular sandwich plate with a non-homogeneous core. 5*th International Conference on Numerical Analysis and Applied Mathematics* (ed. Simos, T. E.), American Institute of Physics, Melville, 364–367 (2007)

[17] MAGNUCKA-BLANDZI, E. Axi-symmetrical deflection and buckling of circular porous-cellular plate. *Thin-Walled Structures*, **46**, 333–337 (2008)

[18] PAWLUS, D. Critical static loads calculations in finite element method of three-layered annular plates. *Archives of Civil and Mechanical Engineering*, **7**, 21–33 (2007)

[19] PAWLUS, D. Critical loads calculations of annular three-layered plates with soft elastic or viscoelastic core. *Archives of Civil and Mechanical Engineering*, **11**, 993–1009 (2011)

[20] ALIPOUR, M. M. and SHARIYAT, M. Analytical zigzag formulation with 3D elasticity corrections for bending and stress analysis of circular/annular composite sandwich plates with auxetic cores. *Composite Structures*, **132**, 175–197 (2015)

[21] MAGNUCKI, K., JASION, P., MAGNUCKA-BLANDZI, E., and WASILEWICZ, P. Theoretical and experimental study of a sandwich circular plate under pure bending. *Thin-Walled Structures*, **79**, 1–7 (2014)

[22] MAO, R., LU, G., WANG, Z., and ZHAO, L. Large deflection behavior of circular sandwich plates with metal foam-core. *European Journal of Mechanics*, **55**, 57–66 (2016)

[23] MOJAHEDIN, A., JABBARI, M., KHORSHIDVAND, A. R., and ESLAMI, M. R. Buckling analysis of functionally graded circular plates made of saturated porous materials based on higher order shear deformation theory. *Thin-Walled Structures*, **99**, 83–90 (2016)